AIAA JOURNAL
Vol. 30, No. 6, June 1992

Adequacy of Modeling Turbulence and Related Effects on Helicopter Response

V. V. George* and G. H. Gaonkar†
Florida Atlantic University, Boca Raton, Florida 33431
and
J. V. R. Prasad‡ and D. P. Schrage§
Georgia Institute of Technology, Atlanta, Georgia 30332

The atmospheric turbulence that a blade station experiences is called blade-fixed turbulence. It can substantially differ from the conventional body-fixed turbulence such as experienced by an element of the body or fuselage because the rotational velocity moves the blade station fore and aft through turbulence. A closed-form solution of a frequency-time spectrum for the dominant vertical turbulence velocity at an arbitrary blade station is developed. This solution explains how and to what extent the rotational velocity affects the frequency and temporal characteristics of the rotor-disk turbulence, such as cyclostationarity, and spectral peaks and split peaks at $1P/2$ or ½ per rev, $1P$, $3P/2$, etc. Comparison of blade flapping response to blade- and body-fixed turbulence is also presented over a range of turbulence scale length and advance ratio: the response statistics comprise frequency-time spectra, correlations, and average threshold-crossing rates. Emphasis is on use of the frequency-time spectra of the cyclostationary turbulence and blade response to predict simultaneously the temporal and frequency characteristics. For low-altitude and low-advance-ratio flights, as in nap-of-the-Earth flights, rotational velocity substantially affects turbulence modeling and, thereby, response statistics.

Introduction

TURBULENCE modeling and related effects on helicopter response, particularly at low altitudes and low speeds, have received renewed attention.[1,2] The state of the art through 1980 is reviewed in Ref. 3; developments since 1980 are covered in Refs. 1, 2, and 4. However, to put this work in perspective, we begin with a brief review of turbulence modeling with rotational velocity effects.

Blade-fixed turbulence that a blade station experiences can differ substantially from the body-fixed turbulence experienced by a nonrotating station such as the center of the rotor disk. This is due to rotational velocity, which moves the blade stations fore and aft through turbulence waves. Turbulence statistics over a time interval depend only on the distance metric or spatial separation relative to the mean wind between the same or two blade stations during that interval; as will be discussed in the next section, this distance, in turn, depends on the rotational velocity as well as the flight velocity.[1,3] The difference between body-fixed turbulence and blade-fixed turbulence was addressed in the 1970s for high-speed compound helicopters (advance ratio $\mu = 1.6$).[5-7] For such high-speed cruising, flight speed nearly five times that of conventional helicopters, the distance metric is virtually determined by the dominant flight speed, as in airplanes, although rotational velocity effects on turbulence modeling are an issue for wind turbines and low-speed helicopters.[4]

That issue for wind turbines was addressed in the pioneering work of Rosenbrock[8] in 1955. Since the 1980s, turbulence modeling for wind turbines has been investigated analytically and experimentally on a sustained basis.[9-12] Figure 1, which is from Ref. 10, shows the correlation between the data and the predicted spectral density of the fore-to-aft turbulence velocity (perpendicular to the turbine disk) for a horizontal axis wind turbine (HAWT) blade station. The predictions are based on the von Kármán model without and with the rotational velocity effects. Because the energy or area under the curve is the same with or without rotational velocity effects, the decrease in energy in the low-frequency region (say, $< 1P/2$ or ½ per rev) is balanced by the increase in energy in the high-frequency region ($> 1P/2$) with the occurrence of peaks at $1P$, $2P$, etc. The monotonically decreasing behavior exhibited by the conventional body-fixed turbulence fails to capture the two basic features of the data: transfer of energy and occurrence of peaks. The blade-fixed turbulence significantly improves the correlation.

Current atmospheric turbulence modeling often fails to acknowledge that rotational velocity effects can be dominant for conventional helicopters ($\mu < 0.4$), particularly for low-advance ratio and low-altitude flights. Accordingly, this investigation advances the state of the art in the following respects:

1) It investigates turbulence and blade response to turbulence, both of which are cyclostationary, by the frequency-time spectra. These spectra simultaneously predict both frequency and temporal characteristics.[13,14] This is noteworthy compared to conventional time-domain correlations,[2-7] which mask the frequency characteristics.

2) It presents a closed-form solution of a frequency-time spectrum of the dominant vertical turbulence excitation at an arbitrary blade station, from which the HAWT model can be recovered for the specialized stationary case. The closed-form solution permits qualitative and parametric investigation of rotational velocity effects on turbulence modeling.

3) It quantifies how blade-fixed turbulence modeling affects the cyclostationary blade response, which is also described by the conventional correlation matrix and average threshold-crossing rates. The emphasis is on low-advance ratio and low-altitude conditions such as nap-of-the-Earth (NOE) flights.

Turbulence Modeling

Following earlier studies,[2-7] we consider only the dominant vertical turbulence velocity component that is nearly normal to the rotor plane, as is the dominant fore-to-aft component for HAWTs. We assume that the rotorcraft experiences

Received May 8, 1991; revision received Sept. 13, 1991; accepted for publication Sept. 14, 1991.

*Research Assistant.
†Professor. Associate Fellow AIAA.
‡Assistant Professor. Member AIAA.
§Professor. Member AIAA.

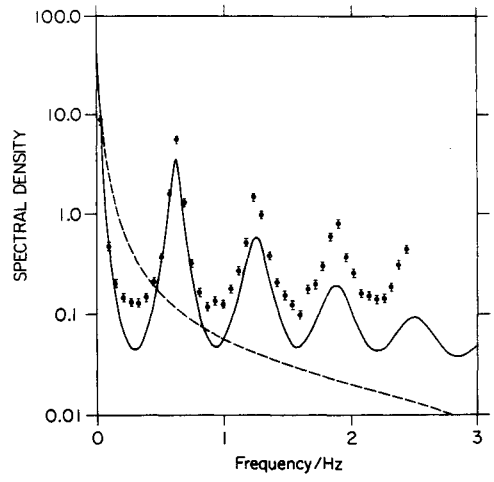

Fig. 1 Von Kármán spectrum of fore-to-aft turbulence seen by a rotating blade station and the center of the turbine disk: Φ experiment; — blade fixed or with rotational velocity effects; --- body fixed or without rotational velocity effects.

homogeneous, isotropic atmospheric turbulence. This implies that the effects of self-induced turbulence, such as those due to downwash and random shedding of trailing vortices, are negligible. We also assume that the Taylor frozen-field approximation applies. For details on the turbulence theory due to von Kármán and Taylor, as applied to rotorcraft, see Refs. 1 and 6.

The spectral densities or the correlations of the turbulence velocity components due to von Kármán are taken as the baseline models. For the vertical component, they are given, respectively, by

$$S_w(\omega_r)/\sigma_w^2 = \frac{L}{2\pi}\frac{[1+(8/3)(1.34L\omega_r)^2]}{[1+(1.34L\omega_r)^2]^{11/6}} \tag{1}$$

$$R_w(r)/\sigma_w^2 = \frac{2}{\Gamma(1/3)}\left[\frac{r}{2.68L}\right]^{1/3}\left[K_{1/3}\left(\frac{r}{1.34L}\right) - \frac{r}{2L}K_{2/3}\left(\frac{r}{1.34L}\right)\right] \tag{2}$$

where L is the scale length of the longitudinal turbulence (that of the vertical turbulence is $L/2$), ω_r is the spatial circular frequency, and $K_{1/3}$ and $K_{2/3}$ are modified Bessel functions of the second kind of fractional order ⅓ and ⅔, respectively. The distance metric r in Eq. (2) discussed next represents the spatial separation relative to the mean wind during the lapsed time or time lag $t_2 - t_1$. A good approximation to the von Kármán model is the exponential model:[2,3]

$$S_w(\omega_r)/\sigma_w^2 = \frac{2L}{\pi}\frac{1}{4+(L\omega_r)^2} \tag{3}$$

$$R_w(r)/\sigma_w^2 = e^{-|r|/(L/2)} \tag{4}$$

We also mention the Rosenbrock model:

$$S_w(\omega_r)/\sigma_w^2 = \frac{L}{4\pi^{1/2}}e^{-(L\omega r)^2/16} \tag{5}$$

$$R_w(r)/\sigma_w^2 = e^{-4r^2/L^2} \tag{6}$$

Though the Rosenbrock model provides only approximate agreement with the von Kármán model, it permits closed-form solution and has been well exploited for wind turbines.[8,9]

Distance Metric r

We consider a rotorcraft flying straight and level, directly into the mean wind, at an airspeed V. If V_{ac} and V_{mw} are ground speeds of the rotorcraft and mean wind, respectively, $V = V_{ac} + V_{mw}$; see Fig. 2. The (X_H, Y_H, Z_H) and (X_B, Y_B, Z_B) systems are the conventional body- or hub-fixed and blade-fixed frames, respectively, in which the Z axis is directed downward and represents both the nonrotating vertical axis Z_H of the hub-fixed system as well as the rotating shaft axis Z_B of the blade-fixed system. Both systems are right handed; whereas the X_H axis represents the flight direction, also referred to as the longitudinal or aft-to-fore direction, the X_B axis along the blade span represents the radial direction. For a blade station at, say, $0.7R$ distance from the center, the velocity components relative to the atmosphere, expressed in inertial or ground-fixed coordinates, are

$$\frac{d}{dt}X_{B/\text{atmosphere}} = \frac{dX}{dt} = V + 0.7\Omega R\sin\Omega t \tag{7}$$

$$\frac{d}{dt}Y_{B/\text{atmosphere}} = \frac{dY}{dt} = 0.7\Omega R\cos\Omega t \tag{8}$$

The magnitude of the distance metric is

$$|r| = [\{X(t_2) - X(t_1)\}^2 + \{Y(t_2) - Y(t_1)\}^2]^{1/2} \tag{9}$$

which is also referred to as the correlation distance. It is convenient to use the following dimensionless time and velocity units:

$$\bar{t}_1 = \Omega t_1, \qquad \bar{t}_2 = \Omega t_2$$
$$\frac{V}{\Omega R(L/2)R} = \frac{\mu}{(L/2R)} = \frac{2\mu}{(L/R)} = a \tag{10}$$

The dimensionless magnitude of the distance metric reduces to

$$\frac{r}{L}(\bar{t}_1,\bar{t}_2) = \frac{1}{2}\left\{a(\bar{t}_2-\bar{t}_1) - 1.4\left(\frac{R}{L}\right)\cos\bar{t}_2 + 1.4\left(\frac{R}{L}\right)\cos\bar{t}_1\right\}^2 + \left\{1.4\left(\frac{R}{L}\right)\sin\bar{t}_2 - 1.4\left(\frac{R}{L}\right)\sin\bar{t}_1\right\}^2\Bigg]^{1/2} \tag{11}$$

We observe that

$$\frac{r}{L}(\bar{t}_1,\bar{t}_2) = \frac{r}{L}(\bar{t}_1 + 2m\pi, \bar{t}_2 + 2n\pi)$$
$$\text{for integer } m = n \text{ only} \tag{12}$$

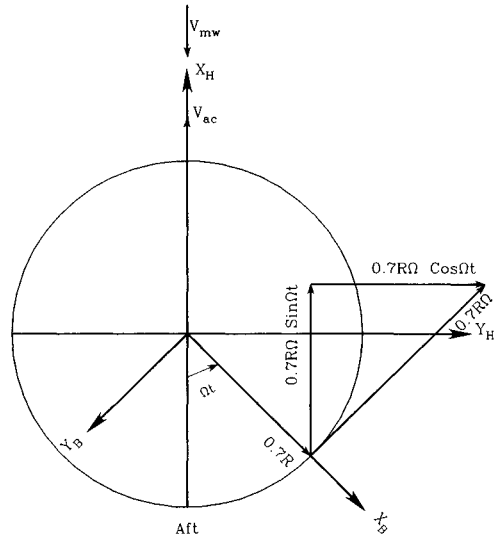

Fig. 2 Blade-fixed and hub-fixed frames with head wind velocity V_{mw}.

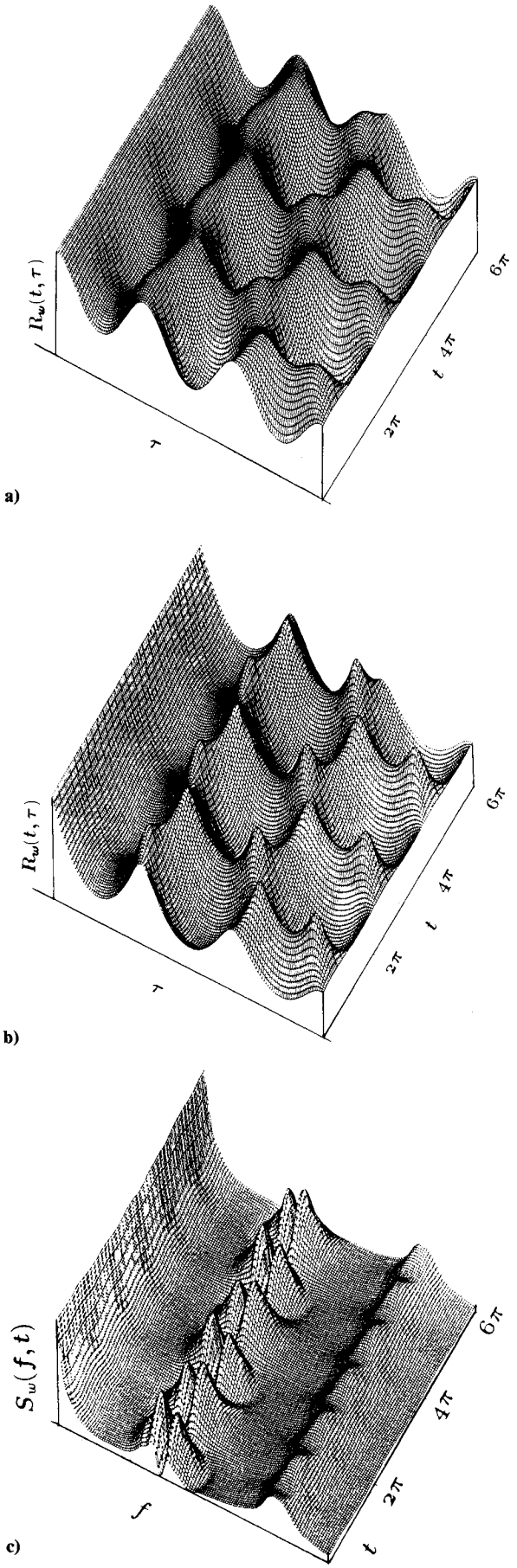

Fig. 3 Perspectives of correlations and frequency-time spectrum of blade-fixed vertical turbulence [$(L/R) = 4$, $\mu = 0.05$]: a) Rosenbrock; b) exponental; c) Rosenbrock.

which shows the periodic structure of the distance metric. As elaborated subsequently, this periodicity has considerable bearing on the stochastic structure of turbulence. With the definitions

$$\bar{t}_2 - \bar{t}_1 = \tau, \qquad \frac{\bar{t}_1 + \bar{t}_2}{2} = t, \qquad c = \frac{1.4}{L/R} \tag{13}$$

the ratio r/L from Eq. (11) takes the form

$$\frac{r}{L}(t,\tau) = \frac{1}{2}\left[\tau^2(a)^2 + 4c \sin\frac{\tau}{2}\left(c \sin\frac{\tau}{2} + a\tau \sin t\right)\right]^{1/2} \tag{14}$$

Substituting this distance metric r/L in Eqs. (2), (4), and (6), we get the correlation functions for the von Kármán, exponential, and Rosenbrock models, respectively.

For later use and referring to Eqs. (10) and (13), we express Eq. (14) as follows:

$$\frac{r}{L}(t,\tau) = \frac{\mu}{L/R}\left[\tau^2 + 4\left(\frac{1.4}{2\mu}\right)^2 \sin^2\frac{\tau}{2} + 4\left(\frac{1.4}{2\mu}\right)\tau \sin\frac{\tau}{2} \sin t\right]^{1/2} \tag{15}$$

Equation (15) shows that the rotational velocity effects or the difference between body-fixed and blade-fixed turbulence should decrease with increasing advance ratio. When rotational velocity effects are neglected, the magnitude of the distance metric simplifies to

$$\left|\frac{r}{L}(t,\tau)\right| = \frac{|a\tau|}{2} \tag{16}$$

As a consequence of Eqs. (12–14), we have

$$R_w(\bar{t}_1 + 2m\pi, \bar{t}_2 + 2n\pi) = R_w(\bar{t}_1, \bar{t}_2), \qquad \text{for } m = n \text{ only} \tag{17}$$

or, equivalently,

$$R_w(t + 2m\pi, \tau) = R_w(t,\tau) \qquad \text{for } m = 0,1,2,\ldots \tag{18}$$

Equation (17) shows that the blade-fixed turbulence belongs to a (wide sense) cyclostationary process.[13–16] However, the process is not mean square periodic since Eq. (18) does not hold for $m \neq n$ (Ref. 13).[13] From Eq. (17), the process is also not (weakly) stationary since $R_w(t_1,t_2)$ is not a function of $t_2 - t_1$ only.[13] Moreover, Eq. (17) or (18) shows that the correlation, though not invariant to arbitrary shifts of $t_2 - t_1$ as in a stationary process, is invariant to shifts of integer multiples of 2π. This nearness to stationarity is better explored by means of frequency-time spectrum or the Wigner distribution.[17,18]

Frequency-Time Spectrum

We assume throughout that the random process $w(t)$ has zero mean. Therefore, the second (joint) moment is equal to the second central moment and the standard deviation $\sigma_w(t)$ or the square root of the variance $\sigma_w^2(t)$ is equal to the rms values. Following Bendat and Pierson,[17] the correlation is defined as

$$R_w(t,\tau) = E[w(t - \tau/2)w(t + \tau/2)] \tag{19}$$

The frequency-time spectrum $S_w(f,t)$ is obtained by taking the Fourier transform of $R_w(t,\tau)$ with respect to τ,

$$S_w(f,t) = \int_{-\infty}^{\infty} R_w(t,\tau)e^{-i2\pi f\tau}\, d\tau \tag{20}$$

Since $R_w(t,\tau)$ is an even function of τ, Eq. (20) simplifies to

$$S_w(f,t) = 2\int_0^{\infty} R_w(t,\tau) \cos 2\pi f\tau\, d\tau \tag{21}$$

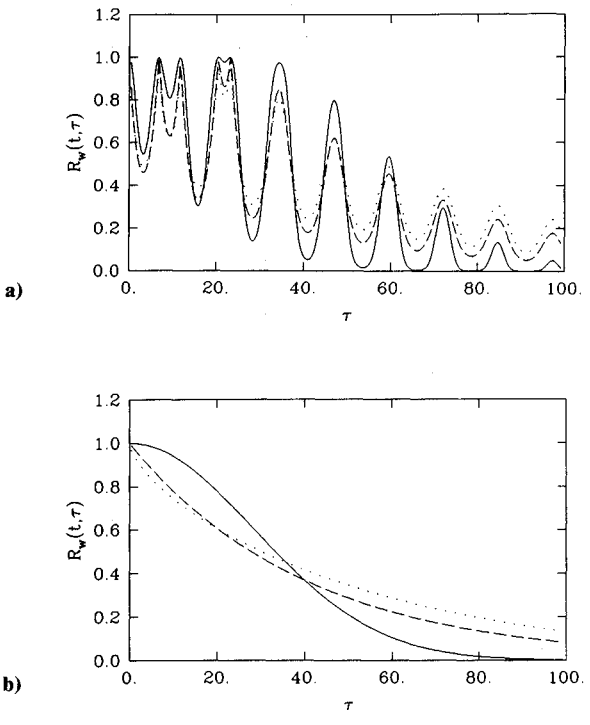

Fig. 4 Comparison of the Rosenbrock correlation with the von Kármán and exponential correlations for vertical turbulence [$\mu = 0.05$; $(L/R) = 4.0$; $t = (2n + \frac{1}{2})\pi$; $n = 0,1,2,\ldots$; — Rosenbrock; --- exponential; · · · von Kármán] a) with rotational velocity effects; b) without rotational velocity effects.

It follows that $S_w(f,t)$ is also real and an even function of f for all values of t. For stationary processes, as in HAWTs and idealized cases of axial flight,[4,9] $S_w(f,t)$ is independent of t and is the conventional power spectral density. In view of Eqs. (18) and (21), we have

$$S_w(f,t) = S_w(f,t + 2m\pi) \tag{22}$$

Thus, $S_w(f,t)$ is periodic with respect to time t. The autocorrelation function $R_w(t,\tau)$ can be obtained by taking the inverse Fourier transform of $S_w(f,t)$:

$$R_w(t,\tau) = \int_{-\infty}^{\infty} S_w(f,t) e^{i2\pi f\tau}\, df \tag{23}$$

For $\tau = 0$, $R_w(t,\tau)$ reduces to the variance

$$\sigma_w^2(t) = E[w^2(t)] = R_w(t,0) = \int_{-\infty}^{\infty} S_w(f,t)\, df \geq 0 \tag{24}$$

Thus, Eq. (24) gives the instantaneous power, a physically appealing feature. Of particular importance are the turbulence concentration or strength at frequency f and turbulence energy in the frequency band $f_2 - f_1$. Therefore, we introduce the temporally averaged (power) spectrum over one rotor revolution $\bar{S}(f)$:

$$\bar{S}(f) = \frac{1}{2\pi}\int_0^{2\pi} S_w(f,t)\, dt \tag{25}$$

as a means of quantifying the turbulence strength at f. We further identify $2\pi\bar{S}(f)$ with the energy spectral density $E[|W(f)|^2]$ at frequency f, where $W(f)$ is the Fourier transform of $w(t)$. Now, the turbulence energy over one rotor revolution in the frequency band $f_2 - f_1$ is quantified by

$$2\pi\int_{f_1}^{f_2} \bar{S}(f)\, df = \int_{f_1}^{f_2}\left[\int_0^{2\pi} S_w(f,t)\, dt\right] df \tag{26}$$

Thus, Eqs. (22), (25), and (26) show why the frequency-time spectral analysis is well suited to cyclostationary processes, although $S(f,t)$ can take negative values.[16-18] Moreover, this spectral representation exploiting cyclostationarity brings out remarkable similarity to the conventional spectral density approach of a stationary process.

Closed-Form Solution

Through Eqs. (1-6), we introduced the von Kármán, exponential, and Rosenbrock models, for which the distance metric r/L is given by Eq. (14). We now give a brief account of the closed-form solution of the frequency-time spectrum for the Rosenbrock model; for details see Refs. 19 and 20.

Rosenbrock Model

The Rosenbrock model is given by

$$R_w(t,\tau) = \exp\left\{-\left(a^2\tau^2 + 4c^2 \sin^2\frac{\tau}{2} + 4ac \sin t\tau \sin\frac{\tau}{2}\right)\right\} \tag{27}$$

Using the notations $A = a$, $4c^2 = B^2$, and $4ac \sin t = C$ we have

$$R_w(t,\tau) = \exp\left\{-A^2\tau^2\right\}\exp\left\{-\left(B^2 \sin^2\frac{\tau}{2} + C\tau \sin\frac{\tau}{2}\right)\right\} \tag{28}$$

After some algebra, it can be shown that[19]

$$R_w(t,\tau) = \sum_{s=0}^{\infty}\sum_{r=s}^{\infty} \frac{(-1)^r}{(r-s)!s!} B^{2s} C^{r-s} \tau^{r-s} e^{-A^2\tau^2} \sin^{r+s}\frac{\tau}{2}$$

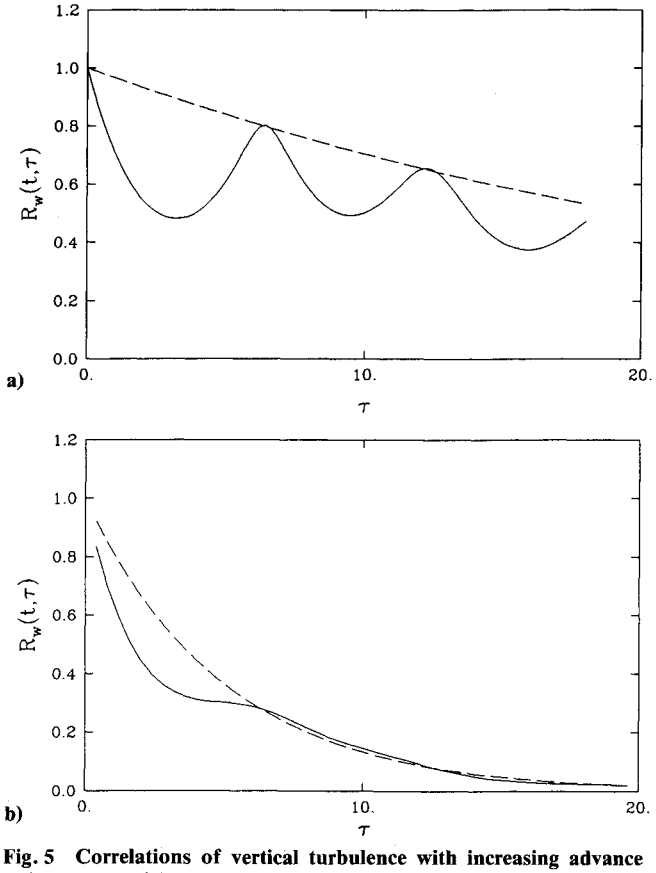

Fig. 5 Correlations of vertical turbulence with increasing advance ratio (exponential model; $L/R = 4$; $t = 0.3$; — blade fixed; --- body fixed): a) $\mu = 0.05$; b) $\mu = 0.4$.

Letting $q = r-s$, this equation reduces to

$$R_w(t,\tau) = \sum_{s=0}^{\infty} \sum_{q=0}^{\infty} \frac{(-1)^{q+s}}{q!s!} B^{2s} C^q \tau^q e^{-A^2\tau^2} \sin^{q+2s}\frac{\tau}{2}$$

In this equation, the last term permits the following series expansion:

$$\sin^{q+2s}\frac{\tau}{2} = \sum_{g=0}^{q+2s}\left[\frac{(-1)^g(q+2s)!(e^{i\tau/2})^{q+2s-g}(e^{-i\tau/2})^g}{(q+2s-g)!g!(2i)^{q+2s}}\right]$$

Let $2u = q + 2s$ and $p = u-g$, then

$$\sin^{2u}\frac{\tau}{2} = \sum_{p=-u}^{p=u} \frac{(-1)^p(2u)!}{2^{2u}(u+p)!(u-p)!} e^{ip\tau}$$

With the following definitions

$$T_1(q) = 1, \quad T_2(q) = 0, \quad \text{for } q = 0,2,4,6, \ldots \text{ even}$$

$$T_1(q) = 1, \quad T_2(q) = 1, \quad \text{for } q = 1,3,5,7, \ldots \text{ odd}$$

the correlation can be expressed as

$$R_w(t,\tau) = \sum_{s=0}^{\infty} \sum_{q=0}^{\infty} \sum_{p=-[(q/2)+s]}^{p=[(q/2)+s]} \times \frac{(-1)^{q+s}(q+2s)!B^{2s}C^q}{2^{q+2s}\, q!s![(q/2)+s+p]![(q/2)+s-p]!} \times \tau^q e^{-A^2\tau^2}\left\{(-1)^p T_1(q) e^{ip\tau} + (-1)^{\frac{2p+1}{2}} T_2(q)\frac{e^{ip\tau}}{i}\right\} \quad (29)$$

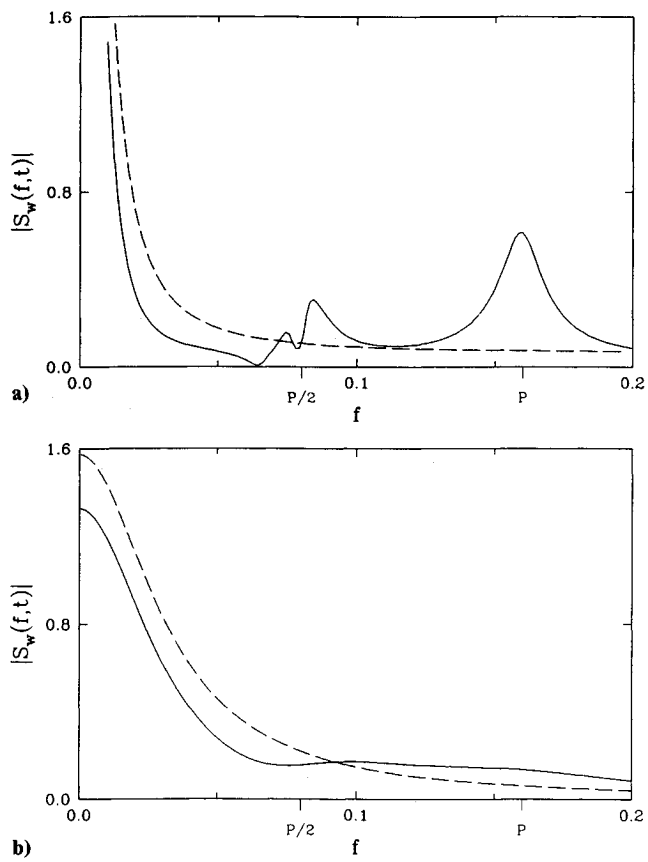

Fig. 6 Frequency-time spectra of vertical turbulence with increasing advance ratio (exponential model; $L/R = 4$; $t = 0.3$; — blade fixed; --- body fixed, spectra divided by 2π): a) $\mu = 0.05$; b) $\mu = 0.4$.

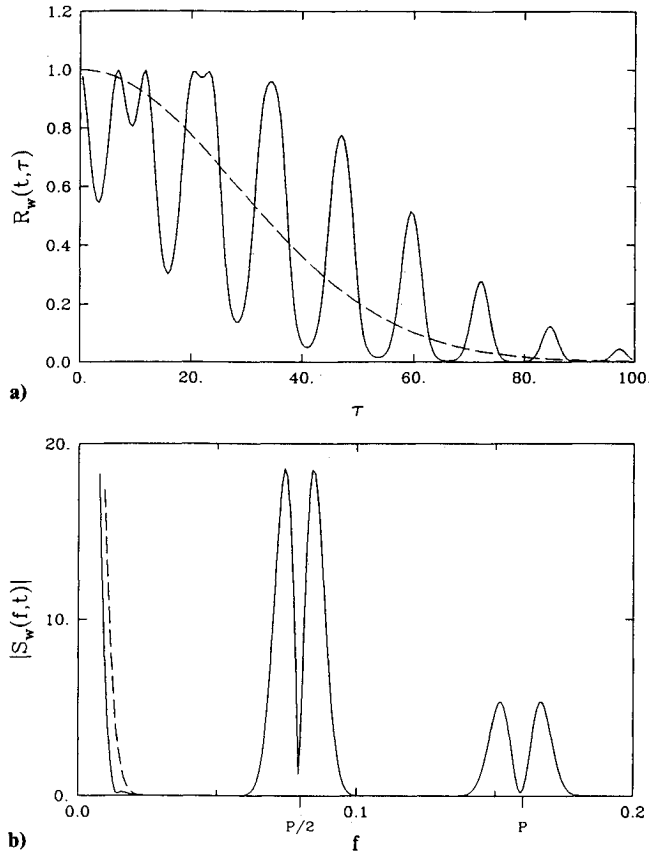

Fig. 7 Correlation and frequency-time spectrum of vertical turbulence for low advance ratio at $t = (2n + \frac{1}{2})\pi$, $n = 0,1,2, \ldots$; (Rosenbrock model; $\mu = 0.05$; $L/R = 4$; — blade fixed; --- body fixed).

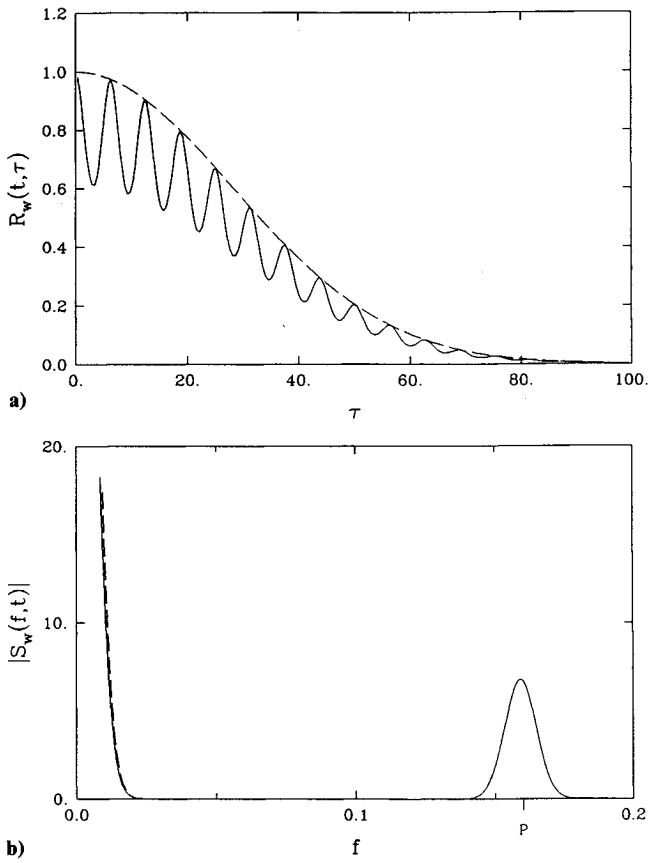

Fig. 8 Correlation and frequency-time spectrum of vertical turbulence for low advance ratio at $t = n = \pi$, $n = 0,1,2, \ldots$; (Rosenbrock model; $\mu = 0.05$; $L/R = 4$; — blade fixed; --- body fixed).

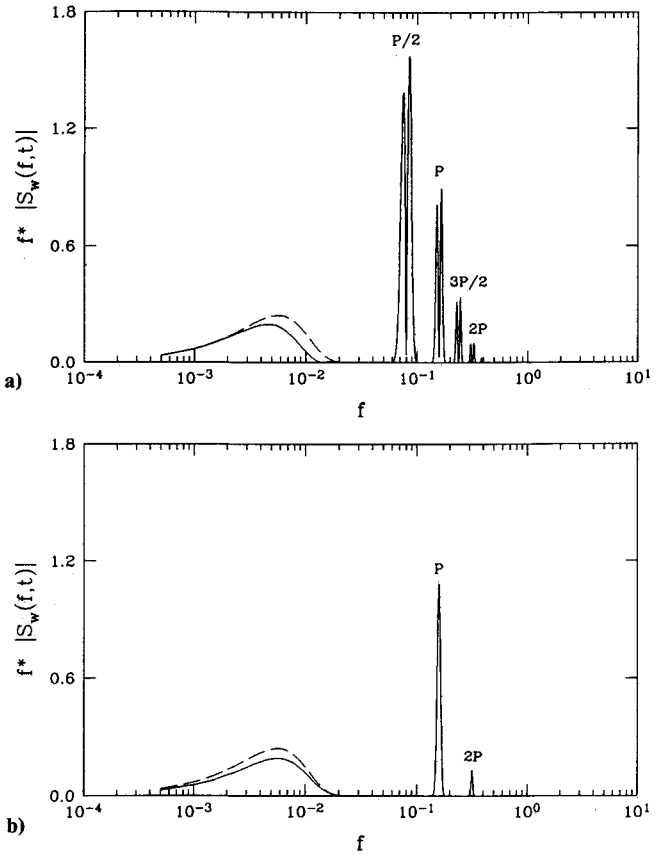

Fig. 9 Frequency-time spectral variation of vertical turbulence (Rosenbrock model; $\mu = 0.05$; $L/R = 4$; — blade fixed; --- body fixed): a) $(2n + 1)\pi/2$; b) $n\pi$.

which is of the form

$$R_w(t,\tau) = I_1(t,\tau) + I_2(t,\tau) \tag{30}$$

Replacing $(e^{ip\tau} + e^{-ip\tau})/2$ by $\cos p\tau$ inside the p summation, we have

$$I_1(t,\tau) = \sum_{s=0}^{\infty} \sum_{q=0}^{\infty} \sum_{p=0}^{p=[(q/2)+s]} \times \frac{(-1)^{q+s}(q+2s)!B^{2s}C^q}{2^{q+2s-1}q!s![(q/2)+s+p]![(q/2)+s-p]!} \times \tau^q e^{-A^2\tau^2} (-1)^p T(p) T_1(q) \cos p\tau$$

where

$$T(p) = 1.0/2.0 \quad \text{if} \quad p = 0$$

$$T(p) = 1.0 \quad \text{if} \quad p = 1,2,\ldots$$

Therefore,[19]

$$I_1(t,\tau) = J_0(t,\tau) + V_1(t,\tau)\cos\tau + V_2(t,\tau)\cos 2\tau + \cdots \tag{31}$$

Replacing $(e^{ip\tau} - e^{ip\tau})/2i$ by $\sin p\tau$ inside the p summation, we have

$$I_2(t,\tau) = \sum_{s=0}^{\infty} \sum_{q=0}^{\infty} \sum_{p=1/2}^{p=[(q/2)+s]} \times \frac{(-1)^{q+s}(q+2s)!B^{2s}C^q}{2^{q+2s-1}q!s![(q/2)+s+p]![(q/2)+s-p]!} \times \tau^q e^{-A^2\tau^2} (-1)^{\frac{2p+1}{2}} T_2(q) \sin p\tau$$

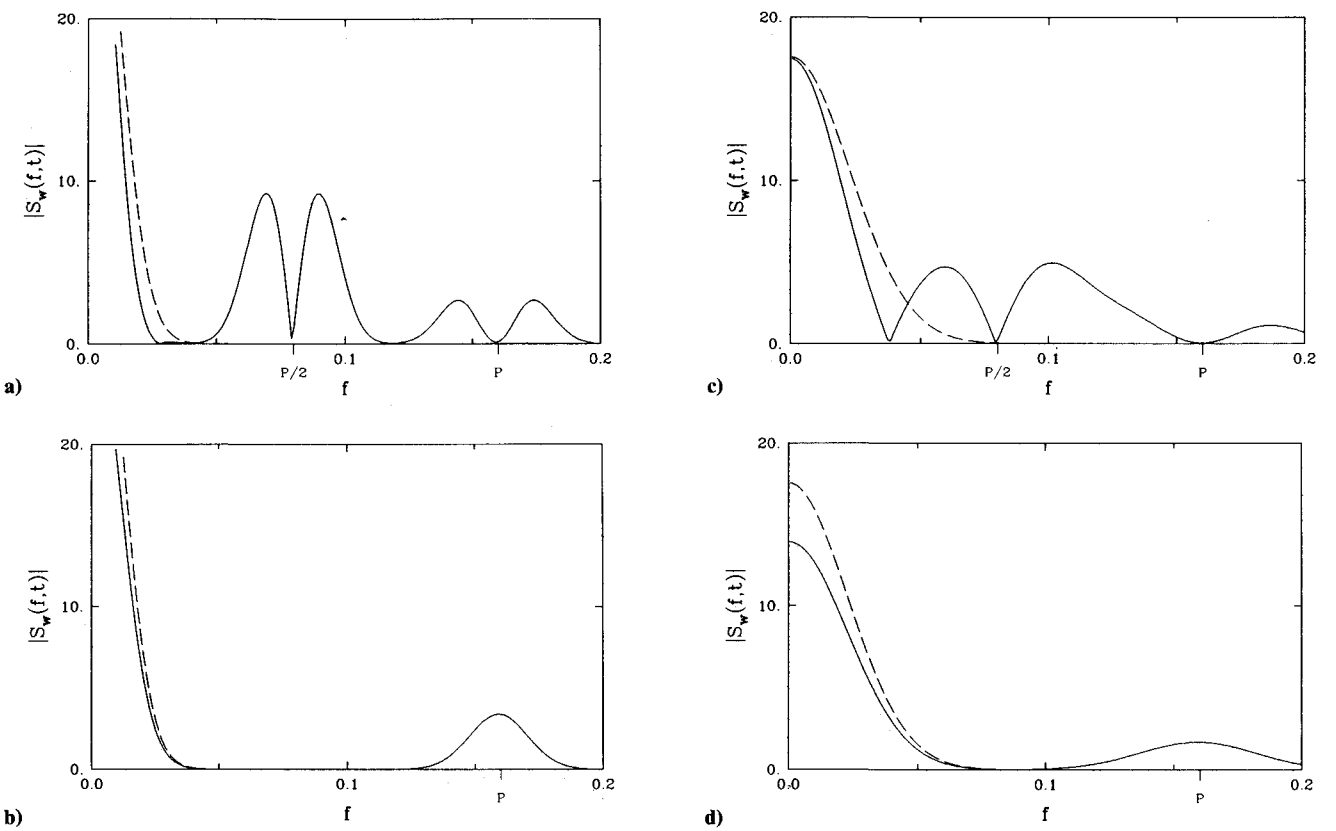

Fig. 10 Frequency-time spectra for different advance ratios and azimuth locations (Rosenbrock model; $L/R = 4$; — blade fixed; --- body fixed): a) $\mu = 0.1$, $t = (2n + \frac{1}{2})\pi$, $n = 0,1,2$; b) $\mu = 0.1$, $t = n\pi$, $n = 0,1,2$; c) $\mu = 0.2$, $t = (2n + \frac{1}{2})\pi$, $n = 0,1,2$; d) $\mu = 0.2$, $t = n\pi$, $n = 0,1,2$.

This equation can also be expressed as

$$I_2(t,\tau) = Z_1(t,\tau)\sin\frac{1}{2}\tau + Z_2(t,\tau)\sin\frac{3}{2}\tau + \cdots \tag{32}$$

Substitution of Eqs. (31) and (32) in Eq. (30) results in

$$R_w(t,\tau) = J_0(t,\tau) + V_1(t,\tau)\cos p\tau + V_2(t,\tau)\cos 2p\tau + \cdots + Z_1(t,\tau)\sin\frac{1}{2}\tau + Z_2(t,\tau)\sin\frac{3}{2}\tau + \cdots \tag{33}$$

Taking the Fourier transform of $R_w(t,\tau)$ with respect to τ, we have the frequency-time spectrum

$$S_w(\omega,t) = \frac{1}{\pi}\int_0^\infty \Big[J_0(t,\tau) + V_1(t,\tau)\cos\tau + V_2(t,\tau)\cos 2\tau + \cdots + Z_1(t,\tau)\sin\frac{1}{2}\tau + Z_2(t,\tau)\sin\frac{3}{2}\tau + \cdots \Big]\cos\omega\tau\, d\tau \tag{34}$$

Let

$$C_0(\omega,t) = \frac{1}{2\pi}\int_{-\infty}^{\infty} J_0(t,\tau)e^{-i\omega\tau}\, d\tau$$

$$C_1(\omega,t) = \frac{1}{2\pi}\int_{-\infty}^{\infty} V_1(t,\tau)e^{-i\omega\tau}\, d\tau$$

$$S_1(\omega,t) = \frac{1}{2\pi}\int_{-\infty}^{\infty} Z_1(t,\tau)e^{-i\omega\tau}\, d\tau$$

$$S_2(\omega,t) = \frac{1}{2\pi}\int_{-\infty}^{\infty} Z_2(t,\tau)e^{-i\omega\tau}\, d\tau$$

Therefore,

$$S_w(\omega,t) = C_0(\omega t) + \frac{C_1(\omega-1,t) + C_1(\omega+1,t)}{2} + \cdots + \frac{S_1[\omega-(1/2),t] + S_1[\omega+(1/2),t]}{2} + \frac{S_2[\omega-(3/2),t] + S_2[\omega+(3/2),t]}{2} + \cdots \tag{35}$$

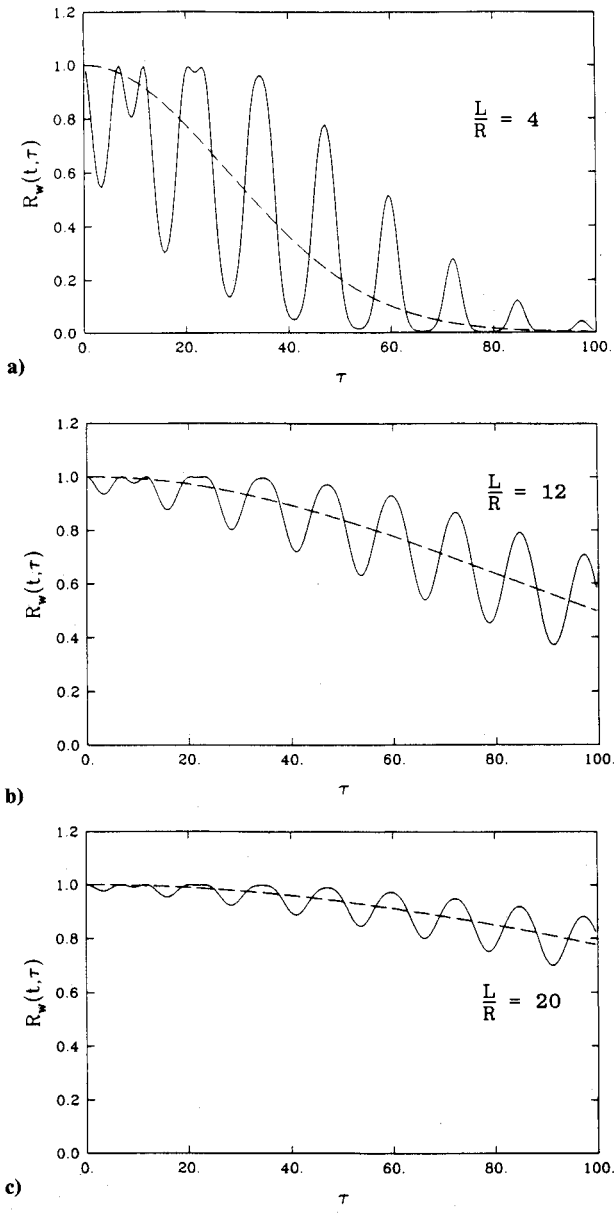

Fig. 11 Vertical turbulence correlations for low advance ratio with increasing turbulence scale length (Rosenbrock model, $\mu = 0.05$; $t = (2n + \frac{1}{2})\pi$; $n = 0,1,2,\ldots$; — blade fixed; --- body fixed): a) $L/R = 4$; b) $L/R = 12$; c) $L/R = 20$.

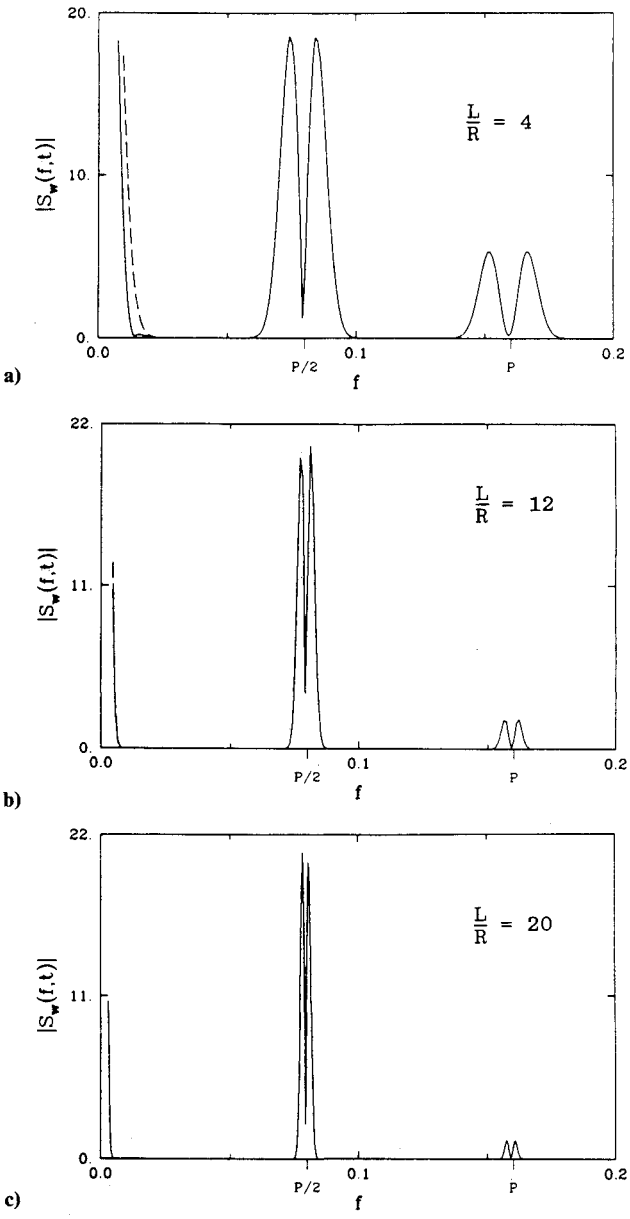

Fig. 12 Vertical turbulence frequency-time spectra for low advance ratio with increasing turbulence scale length (Rosenbrock model, $\mu = 0.05$; $t = (2n + \frac{1}{2})\pi$; $n = 0,1,2,\ldots$; — blade fixed; --- body fixed): a) $L/R = 4$; b) $L/R = 12$; c) $L/R = 20$.

Equation (35) is instructive in that the variation of $S_w(\omega,t)$ for instantaneous azimuth locations has preferred locations at $1P/2$, $1P$, $3P/2$, etc., a feature that will be further explored on the basis of numerical results. Replacing J_0, V_1, . . . and Z_1, Z_2, . . . with the corresponding series sums, we get

$$S_w(\omega,t) = \frac{1}{\pi} \sum_{s=0}^{\infty} \sum_{q=0}^{\infty} \sum_{p=-[(q/2)+s]}^{p=[(q/2)+s]} \times \frac{(-1)^{q+s}(q+2s)!B^{2s}C^q}{2^{q+2s}\, q!s![(q/2)+s+p]![(q/2)+s-p]!} \times \int_0^{\infty} \tau^q e^{-A^2\tau^2} \{(-1)^p T_1(q) \cos(\omega+p)\tau + (-1)^{\frac{2p+1}{2}} T_2(q) \sin(\omega+p)\tau\}\, d\tau \tag{36}$$

The integral of Eq. (36) can be represented in terms of the following degenerative hypergeometric function[21]:

$$\Phi(\nu,\kappa;Z) = 1 + \frac{\nu}{\kappa} Z + \frac{\nu(\nu+1)}{\kappa(\kappa+1)} \frac{Z^2}{2!} + \frac{\nu(\nu+1)(\nu+2)}{\kappa(\kappa+1)(\kappa+2)} \frac{Z^3}{3!} + \cdots \tag{37}$$

which satisfies the following identities:

$$\int_0^{\infty} x^{\eta-1} e^{-\beta x^2} \cos mx\, dx = \frac{\Gamma(\eta/2)}{\beta^{\eta/2}} \Phi\left(\frac{\eta}{2}; \frac{1}{2}; -\frac{m^2}{4\beta}\right) \tag{38}$$

$$\int_0^{\infty} x^{\eta-1} e^{-\beta x^2} \sin mx\, dx = \frac{m e^{-(m^2/4\beta)}}{2\beta^{(\eta+1)/2}} \Gamma\left(\frac{\eta+1}{2}\right) \Phi\left(1-\frac{\eta}{2}; \frac{3}{2}; \frac{m^2}{4\beta}\right) \tag{39}$$

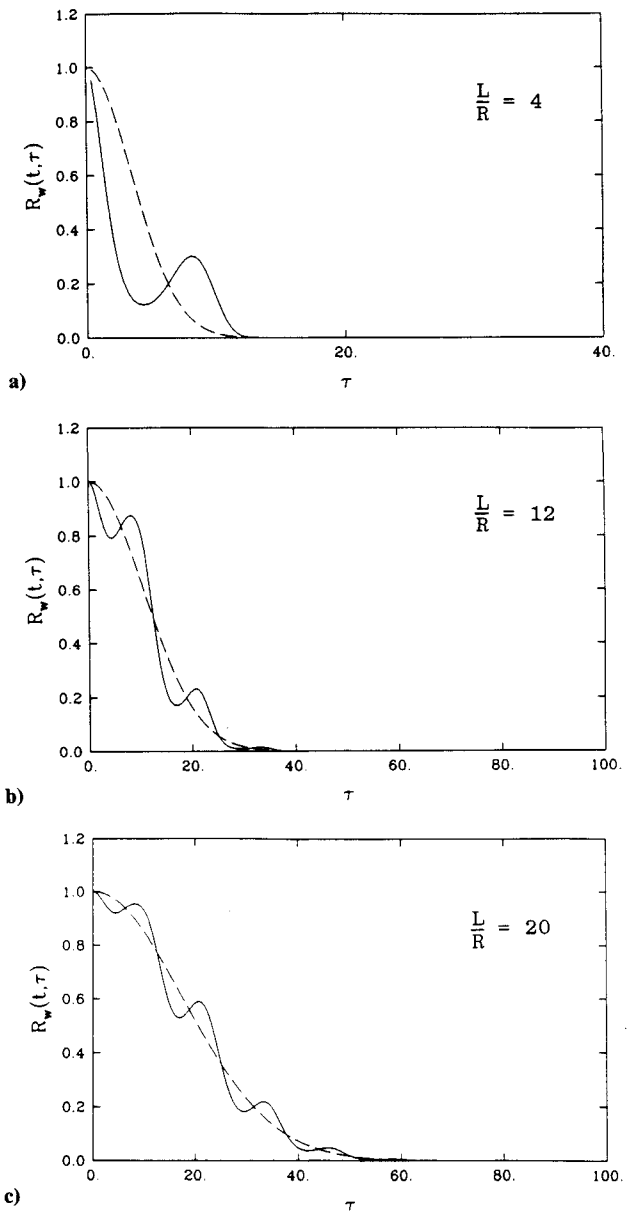

Fig. 13 Vertical turbulence correlations for high advance ratio with increasing turbulence scale length (Rosenbrock model, $\mu = 0.4$; $t = (2n + \frac{1}{2})\pi$; $n = 0,1,2,\ldots$; — blade fixed; --- body fixed): a) $L/R = 4$; b) $L/R = 12$; c) $L/R = 20$.

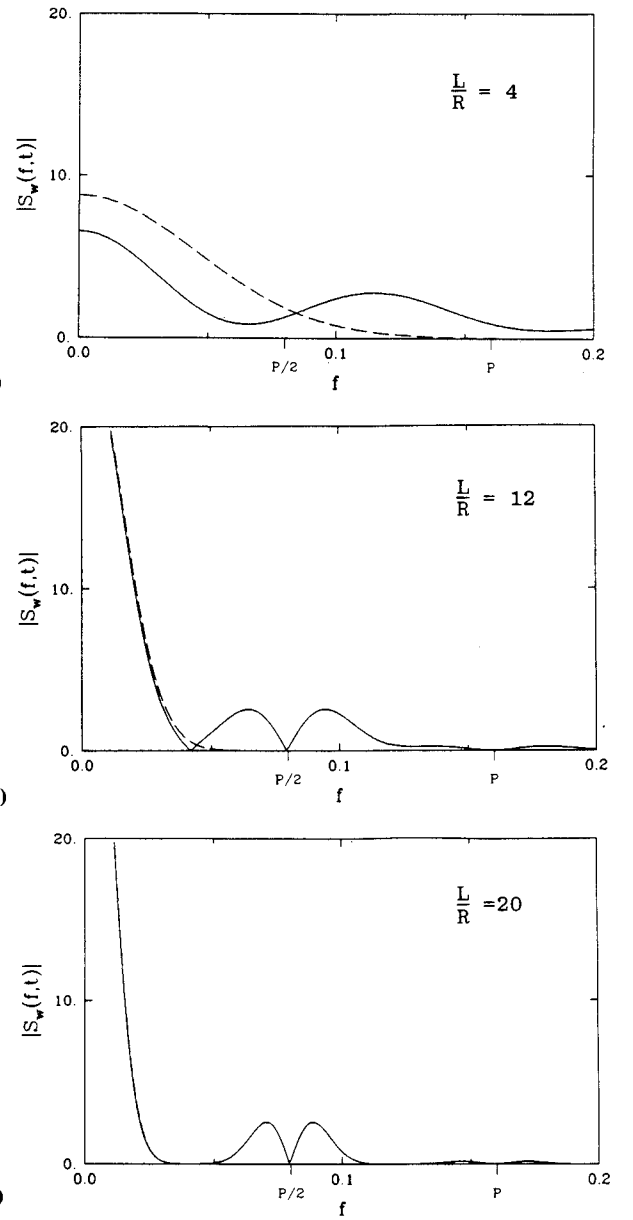

Fig. 14 Vertical turbulence frequency-time spectra for high advance ratio with increasing turbulence scale length (Rosenbrock model, $\mu = 0.4$; $t = (2n + \frac{1}{2})\pi$; $n = 0,1,2,\ldots$; — blade fixed; --- body fixed): a) $L/R = 4$; b) $L/R = 12$; c) $L/R = 20$.

Substituting Eqs. (38) and (39) in Eq. (36), we get

$$S_w(\omega,t) = \frac{1}{\pi}\sum_{s=0}^{\infty}\sum_{q=0}^{\infty}\sum_{p=-[(q/2)+s]}^{p=[(q/2)+s]} \times \frac{(-1)^{q+s}(q+2s)!B^{2s}C^q}{2^{q+2s}\,q!s![(q/2)+s+p]![(q/2)+s-p]!} \times \left\{(-1)^p T_1(q)\frac{\Gamma[(q+1)/2]}{2A^{q+1}}\Phi\left(\frac{q+1}{2},\frac{1}{2};\frac{-(\omega+p)^2}{4A^2}\right)\right.$$

$$+(-1)^{\frac{2p+1}{2}}T_2(q)\frac{(\omega+p)\exp[-(\omega+p)^2/4A^2]}{2A^{q+2}} \times \left.\Gamma\left(\frac{q+1}{2}\right)\Phi\left(\frac{1-q}{2},\frac{3}{2};\frac{(\omega+p)^2}{4A^2}\right)\right\} \quad (40)$$

That is,

$$S_w(\omega,t) = [N_1(\omega,t) + N_2(\omega,t) + \cdots] + [L_1(\omega,t) + L_2(\omega,t) + \cdots] = [M_1(\omega,t)] + [M_2(\omega,t)] \quad (41)$$

We observe that $M_1(\omega,t)$ and $M_2(\omega,t)$ are the Fourier transforms of $I_1(t,\tau)$ and $I_2(t,\tau)$, respectively, with respect to τ.

Turbulence Statistics

The statistics comprise the correlation and frequency-time spectral density of the vertical turbulence velocities at the $0.7R$ blade station. The following parameters are assumed: $0.05 \le \mu \le 0.8$, $4.0 \le L/R \le 20.0$. For conventional pure helicopters, the advance ratio is close to 0.35. Moreover, up to altitudes of 500 ft, the so-called planetary boundary layer, the turbulence scale length is of the same order of magnitude as the rotor radius; at higher altitudes, it increases with increasing altitude.[1] For a rotor, say with 35-ft radius, the value $L/R = 4.0$ is typical of altitudes 400 ft and below. The correlation statistics in the t-τ plane are based on the Rosenbrock, exponential, and von Kármán models, characterized by Eqs. (2), (4), and (6), respectively. In each model, the distance metric r/L is given by Eq. (14) when rotational velocity effects are included and by Eq. (16) when these effects are neglected. Choice of the f-t plane is motivated by the wind-turbine experience (see Fig. 1): rotational velocity effects, masked in the conventional time-domain description, dominate the frequency characteristics. The frequency-time description is based on the closed-form and numerical solutions of the frequency-time spectral density for the Rosenbrock and exponential models, respectively. The objective is to predict the rotational velocity effects on turbulence modeling with respect to flight speed μ and turbulence scale length L/R.

Figure 3 shows perspectives of the correlation and frequency-time spectral density for the Rosenbrock model and the correlation for the exponential model: $\mu = 0.05$ and $L/R = 4$. The correlations show qualitative agreement between

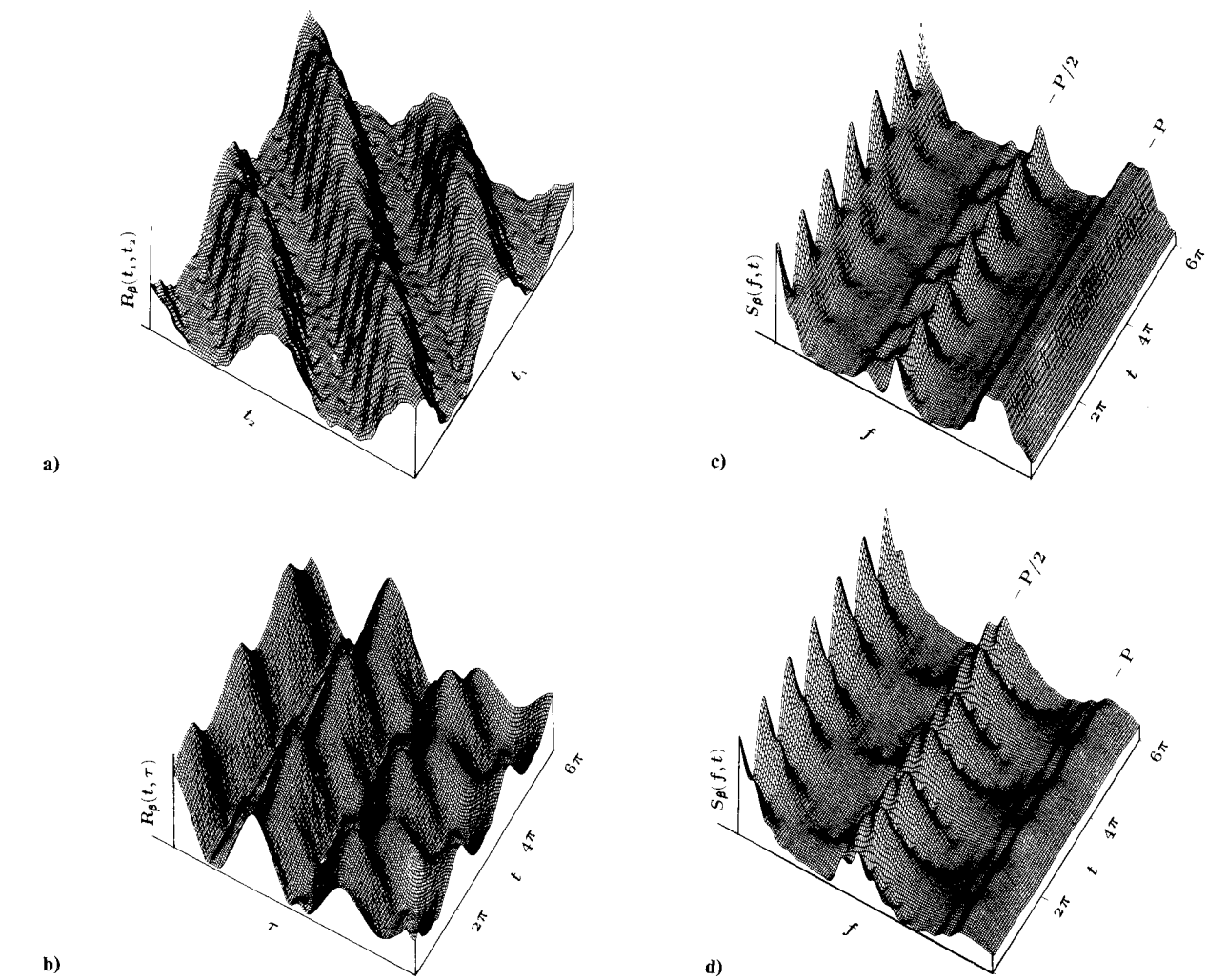

Fig. 15 Perspectives of flapping response correlations and frequency-time spectra ($L/R = 4$; $p = 1.1$; $\gamma = 4$): a) $\mu = 0.05$; b) $\mu = 0.05$; c) $\mu = 0.05$; d) $\mu = 0.2$.

the two models such as decay with increasing elapsed time τ. Moreover, both the correlation and spectral density show periodicity along the t axis. This perodicity demonstrates the similarity as well as the dissimilarity between cyclostationary rotorcraft turbulence and conventional stationary turbulence, as in airplanes and HAWTs. That is, the rotorcraft turbulence statistics are not time invariant for arbitrary time shifts as in a stationary process but are, nevertheless, invariant for time shifts of integer multiples of rotor revolution; see Eqs. (17), (18), and (22). Concerning the description in the f-t plane, mention must be made of peaks and split peaks at $1P/2$ and $1P$; see Eq. (35). A qualitative application of Eqs. (25) and (26) to the perspective of frequency-time spectrum in Fig. 3 is revealing. This shows that the turbulence "strength" is concentrated within preferred frequency bands centered on $P/2$ and P, the latter concentration near P is analogous to the wind-turbine experience; see Fig. 1. We reiterate that, whereas

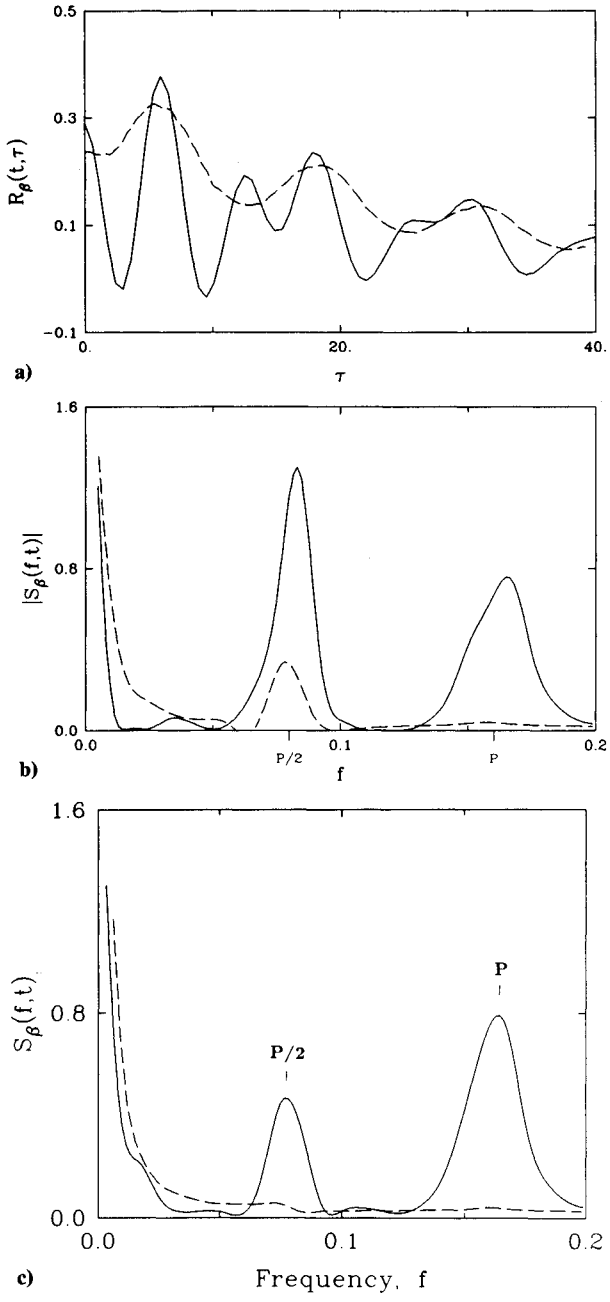

Fig. 16 Flapping response correlation and frequency-time spectra at low advance ratio ($L/R = 4$; $\mu = 0.05$; $p = 1.1$; $\gamma = 4$; — blade-fixed turbulence excitation; --- body-fixed turbulence excitation): a) $t = 0.3$; b) $t = 0.3$; c) $t = 1.15$.

the rotorcraft turbulence is cyclostationary, the HAWT turbulence is stationary. The statistics are further elaborated in Fig. 4 for the blade azimuth locations of $t = (2n + \frac{1}{2})\pi$, $n = 0,1,2,\ldots$; correlations are based on the Rosenbrock, exponential, and von Kármán models; Fig. 4a includes rotational velocity effects, and Fig. 4b neglects them. The exponential model provides good approximation to the baseline von Kármán model without and with the rotational velocity effects. By comparison, the Rosenbrock model fairly agrees with the other two. All three models demonstrate that the rotational velocity effects introduce substantial changes in the turbulence statistics. Overall, the Rosenbrock model is viable in establishing trends of the rotational velocity effects on turbulence modeling.

Figures 5 and 6 give an overview of turbulence statistics based on the exponential model; both low-speed ($\mu = 0.05$) and high-speed ($\mu = 0.4$) conditions are considered. The results are for $L/R = 4$ at an arbitrary time $t = 0.3$. The correlation of Fig. 5 shows that the rotational velocity effects decrease with increasing advance ratio, as discussed earlier on the basis of Eq. (15). The frequency-time spectrum of Fig. 6 also shows, as expected, that the rotational velocity effects decrease with increasing advance ratio. More significantly, the spectral density results demonstrate simultaneous prediction of frequency- and time-dependent features such as the occurrence of peaks and split peaks at $1P/2$ and $1P$, etc., for arbitrary azimuthal or temporal positions of the blade. We further explore the rotational velocity effects on turbulence modeling on the basis of the Rosenbrock model, Eqs. (28), (35), and (40); particularly, the closed-form solution of the frequency-time spectral density facilitates analytical and parametric investigations in the f-t plane.

Figures 7–10 show both the correlation and frequency-time spectral density for a turbulence scale length of $L/R = 4.0$. They demonstrate the rotational velocity effects on turbulence modeling with increasing flight speed, $0.05 \le \mu \le 0.4$. For each case, we consider two azimuth locations: $t = (2n + 1)\pi/2$ and $t = n\pi$, $n = 0,1,2,\ldots$. Figure 7 shows that neglect of rotational velocity effects leads to incorrect prediction of turbulence statistics and can adversely affect prediction of helicopter response statistics. The correlation $R_w(t,\tau)$ for $t = (2n + 1)(\pi/2)$ oscillates almost evenly about the stationary case obtained by neglecting the rotational velocity effects. For the azimuth locations $t = n\pi$, $n = 0,1,2,\ldots$, Fig. 8 shows the correlation and spectral density with and without rotational velocity effects. The results are similar to the stationary cases of the HAWTs and idealized axial flights.[4,8–12] This similarity is expected because for $t = n\pi$, $n = 0,1,2,\ldots$, $\sin t$ in Eq. (14) vanishes; Z_1 and Z_2 terms in Eq. (33) and S_1, S_2 terms in Eq. (35) disappear. Compared with Fig. 7, the results differ in three respects. First, the consistent overshoot above the stationary value is absent; the body-fixed correlation forms an amplitude envelope to the stationary blade-fixed correlation. Second, the split peaks at $1P/2$, $3P/2$, etc., disappear and the frequency-time spectrum is concentrated at $1P$, $2P$, etc. Third, rotational velocity effects, though appreciable, are relatively less severe.

Of particular importance in handling qualities and fatigue are the frequencies around which the excitation is dominant. This point is further explored in Fig. 9, in which spectral density results of Figs. 7 and 8 are presented in a semilog scale, $f*S(f,t)$ vs f. In this scale, spectral density presentation of Figs. 7 and 8 provides a sharper focus on the low-frequency region. Conventional body-fixed modeling cannot predict the peaks at $1P/2$, $1P$, etc. Thus, the turbulence excitation in the high-frequency region is rapidly attenuated and the gust response of high-frequency blade modes is expected to be underpredicted. For $L/R = 4$, Fig. 10 for $\mu = 0.1$ and 0.2 shows essentially the same trends as Fig. 6 for $\mu = 0.05$ and 0.4 and Figs. 7b and 8b for $\mu = 0.05$, the occurrence of peaks in spectral density variation because of rotational velocity effects that decrease with increasing speed μ.

Figures 11–14 show the rotational velocity effects on turbulence statistics with increasing turbulence scale length. In each figure, $L/R = 4$, 12, and 20 and $t = (2n + \frac{1}{2})\pi$, $n = 0,1,2,\ldots$; Figs. 11 and 12 show the low-advance ratio case with $\mu = 0.05$, and Figs. 13 and 14, the high advance-ratio case with $\mu = 0.4$. All four figures show that the rotational velocity effects decrease with increasing turbulence scale length. This is expected since the spatial wave length of turbulence waves is of the same order of magnitude as the scale length. In such high scale-length gust encounters, say, as typified by $L/R = 20$, the rotor radius is far less than the wave length and a blade station essentially sees uniform turbulence. Finally, we compare Figs. 11 and 12 with Figs. 13 and 14. These comparisons show that for a typical helicopter, say, with a rotor radius of 35 ft and $\mu = 0.3$, rotational velocity effects are not negligible for low-altitude flights, say, $L/R \leq 12.0$.

Response Statistics

When linearized about a periodic forced response, the blade response to cyclostationary turbulence is also cyclostationary, as typified by Eqs. (17) and (18).[19,20] The mathematical model represents a rigid root-restrained blade executing flapping motion $\beta(t)$. The root-spring stiffness, blade mass distribution, and rotor rotational speed provide a normalized rotating flapping frequency p and lock number γ. The aerodynamic representation is based on both the linear quasisteady aerodynamics and unified dynamic stall lift theories.[20] However, the subsequent discussion of numerical results assumes quasisteady aerodynamics. Concerning the basic issue of turbulence modeling with or without rotational velocity effects, both sets of results demonstrate the same qualitative aspects. For numerical results based on unified dynamic stall lift theory, see Refs. 20 and 22. The flapping response statistics comprise correlation $R_{\beta\beta}(t_1,t_2)$ as well as $R_{\beta\beta}(t,\tau)$, frequency-time spectrum $S_\beta(f,t)$, and also zero-level threshold upcrossing rate $E[N_{+\beta}(0,t)]$. For additional results on standard deviations of flapping σ_β, flapping rate $\sigma_{\dot\beta}$, correlation coefficient between flapping and flapping rate $\rho_{\beta\dot\beta}$, and threshold upcrossing rates $E[N_{+\beta}(\eta,t)]$ for different threshold levels η, see Refs. 20 and 22. The turbulence excitation is based on the exponential model. For additional details on response frequency-time spectra, see Refs. 14–17, and on response correlation including threshold upcrossings, see Refs. 2 and 4.

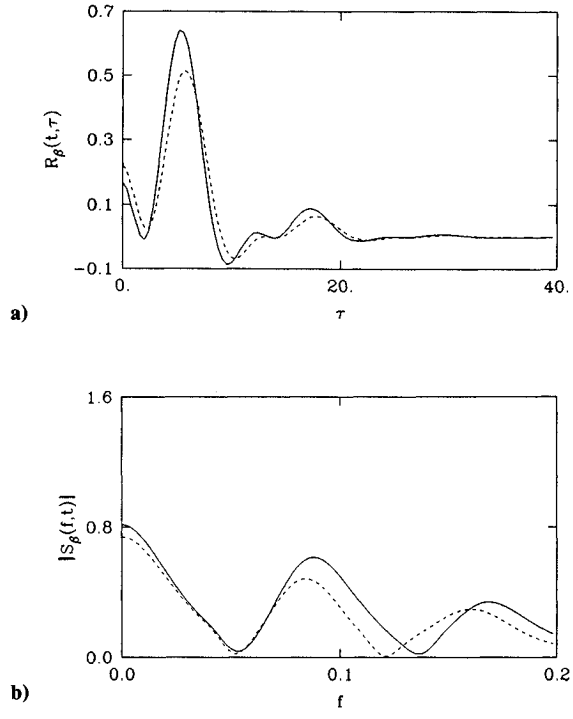

Fig. 17 Flapping response correlation and frequency-time spectra at high advance ratio ($L/R = 4$; $\mu = 0.4$; $p = 1.1$; $\gamma = 4$; — blade-fixed turbulence excitation; --- body-fixed turbulence excitation): a) $t = 0.3$; b) $t = 0.3$.

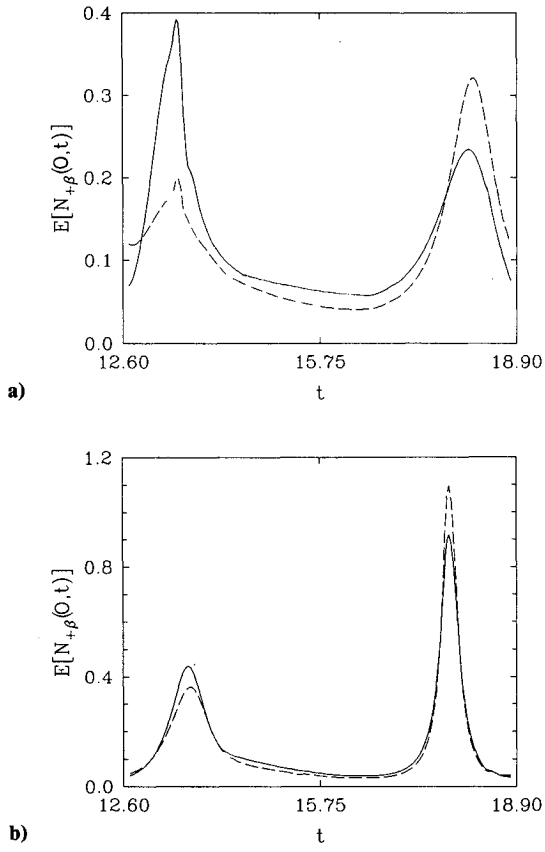

Fig. 18 Average zero-level crossing rates of flapping response with increasing advance ratio ($L/R = 4$; $p = 1.1$; $\gamma = 4$;— blade-fixed turbulence excitation; --- body-fixed turbulence excitation): a) $\mu = 0.4$; b) $\mu = 0.8$.

We investigate how rotational velocity effects on turbulence modeling affect blade response prediction. The following parameter ranges are used: $0.05 \leq \mu \leq 0.8$, $4.0 \leq L/R \leq 20.0$, $p = 1.1$, $\gamma = 4$. Figure 15 shows perspectives of the correlations $R_\beta(t_1,t_2)$ and $R_\beta(t,\tau)$ for $\mu = 0.05$ and frequency-time spectral density $S_\beta(f,t)$ for $\mu = 0.05$ and 0.2 of the flapping response. The correlations $R_\beta(t_1,t_2)$ along the diagonal $t_1 = t_2$ or $R_\beta(t,\tau)$ for $\tau = 0$ represent the variance $\sigma_\beta^2(t)$, which exhibits perodicity. Similar to the excitation, the response correlation (f,t) show rapid decay along the τ axis and perodicity along the t axis, and $S_\beta(f,t)$ also shows peaks around $1P/2$ and $1P$.

Figure 16 shows the correlation $R_\beta(t,\tau)$ for $t = 0.3$ and spectral density $S_\beta(f,t)$ for $t = 0.3$ and 1.15; for each case, $\mu = 0.05$. The temporal values of $t = 0.3$ and 1.15 are somewhat arbitrarily chosen and correspond to azimuth locations of 17 and 86 deg from the aft position. We clearly see the dominant influence of rotational velocity effects on response correlation and spectral density, qualitatively affecting both temporal and frequency characteristics. The spectral peaks around $1P/2$ and $1P$ when rotational velocity effects on turbulence modeling are included and appreciable attenuation of such peaks when the effects are neglected merit attention. With increasing μ, the rotational velocity effects on turbulence modeling and, in turn, on response decrease. This point is well borne out by a comparison of Fig. 17 for $\mu = 0.4$ with Fig. 16 for $\mu = 0.05$; for both figures $L/R = 4$.

Figure 18 shows the average or the expectation of the upcrossing rate of the zero level by the flapping oscillations. The expectation rate of threshold upcrossings of $\beta(t)$ depends on the three response components, $\sigma_\beta(t)$, $\sigma_{\dot\beta}(t)$, and $\rho_{\beta\dot\beta}(t)$, for

which the rotational velocity effects decrease with increasing advance ratio.[19,20] This is well corroborated by Fig. 18a for $\mu = 0.4$. At $\mu = 0.8$, the system is typical of compound helicopters, when rotational velocity effects on turbulence modeling and in turn on response cease to be an issue.

Conclusions

The frequency-time spectra are well suited to investigate the turbulence and helicopter response to turbulence, both of which are cyclostationary or nearly stationary. They show both the frequency and temporal features for varying frequency at discrete times as well as for varying time at discrete frequencies. This brings out the closeness of the cyclostationary turbulence and blade response processes to a stationary process. These features facilitate the prediction and interpretation of fatigue, and low- and high-frequency vibrations.

This study also leads to the following conclusions:

1) The developed closed-form solution of the frequency-time turbulence spectrum provides a qualitative and parametric investigation of the turbulence characteristics with respect to frequency and time; earlier investigated wind-turbine cases can be treated as special stationary cases. This significantly facilitates investigation of rotational velocity effects on turbulence modeling, showing the turbulence frequency-time spectral concentration as sharp peaks within preferred frequency bands centered on $1P/2$, $1P$, $3P/2$, etc. By contrast, the conventional body-fixed turbulence modeling suppresses such peaks with rapid attenuation of such peaks with increasing frequency. This may lead to erroneous prediction of low-frequency handling qualities characteristics and high-frequency loads and vibrations.

2) The response statistics comprising frequency-time spectra and the conventional correlations including average threshold upcrossing rates are significantly affected by the rotational velocity effects on turbulence modeling, which decrease with increasing advance ratio and turbulence scale length. For conventional helicopters (advance ratio $\mu < 0.4$) operating at altitudes of 1000 ft or below (say, $L/R < 12$), the rotational velocity effects are not negligible. This means that, for NOE flights, rotational velocity effects on turbulence modeling should be included.

Acknowledgments

This work is sponsored by the Aeroflightdynamics Directorate at NASA Ames Research Center under NASA Ames University consortium interchange NCA 2-512. We are grateful to K. H. Hohenemser of Washington University for his comments.

References

[1]Costello, M. F., "A Theory for the Analysis of Rotorcraft Operating in Atmospheric Turbulence," *Proceedings of the American Helicopter Society 46th Annual National Forum,* Vol. 2, American Helicopter Society, Washington, DC, 1990, pp. 1003–1015.

[2]Elliot, A. S., and Chopra, I., "Helicopter Response to Atmospheric Turbulence in Forward Flight," *Journal of the American Helicopter Society,* Vol. 35, No. 2, 1990, pp. 51–59.

[3]Gaonkar, G. H., "Gust Response of Rotor and Propeller Systems," *Journal of Aircraft,* Vol. 18, No. 5, 1981, pp. 389–396.

[4]Gaonkar, G. H., "A Perspective on Modeling Rotorcraft in Turbulence," *Probabilistic Engineering Mechanics Journal,* Vol. 3, No. 1, 1988, pp. 36–42.

[5]Gaonkar, G. H., and Hohenemser, K. H., "An Advanced Stochastic Model for Threshold Crossing Studies of Rotor Blade Vibrations," *AIAA Journal,* Vol. 10, No. 8, 1972, pp. 1100, 1101.

[6]Gaonkar, G. H., and Hohenemser, K. H., "Comparison of Two Stochastic Models for Threshold Crossing Studies of Rotor Blade Vibrations," AIAA/ASME 12th Structures, Structural Dynamics, and Materials Conference, AIAA Paper 71-389, Anaheim, CA, April 1971.

[7]Gaonkar, G. H., "Random Vibration Peaks in Rotorcraft and the Effects of Nonuniform Gusts," *Journal of Aircraft,* Vol. 14, No. 1, 1977, pp. 68–76.

[8]Rosenbrock, H. H., "Vibration and Stability Problems in Large Wind Turbines Having Hinged Blades," British Electrical and Allied Industries Research Association, TR C/T 113, Surrey, England, UK, 1955, pp. 1–53.

[9]Connell, J. R., "The Spectrum of Wind Speed Fluctuations Encountered by a Rotating Blade of Wind Energy Conversion System," *Solar Energy,* Vol. 29, No. 5, 1982, pp. 363–375.

[10]Anderson, M. B., and Fordham, E. J., "An Analysis of Results From an Atmospheric Experiment to Examine the Structure of the Turbulent Wind As Seen by a Rotating Observer," Univ. of Cambridge, Cavendish Lab. Rept., Cambridge, England, UK, 1982.

[11]Connell, J. R., and Morris, V. R., "Turbulent Wind at the Equatorial Segment of an Operating Darrieus Wind Turbine Blade," *Ninth ASME Wind Energy Symposium,* SED-Vol. 9, American Society of Mechanical Engineers, New York, 1988, pp. 25–31.

[12]Dragt, J. B., "Atmospheric Turbulence Characteristics in the Rotating Frame of Reference of a WECS Rotor," European Community Wind Energy Conference (ECWEC), Madrid, Sept. 1990.

[13]Papoulis, A., *Probability, Random Variables and Stochastic Processes,* McGraw-Hill, New York, 1984, Chap. 9.

[14]Gardner, W., *Statistical Spectral Analysis,* Prentice-Hall, Englewood Cliffs, NJ, 1988, Chap. 10.

[15]Ogura, H., "Spectral Representation of a Periodic Nonstationary Process," *IEEE Transactions on Information Theory,* Vol. IT-17, No. 2, 1971, pp. 143–149.

[16]Gardner, W. A., *Introduction to Random Processes,* McGraw-Hill, St. Louis, MO, 1990, Chap. 12.

[17]Bendat, J. S, and Piersol, A. G., *Random Data,* Wiley, New York, 1986, Chap. 12.

[18]Claasen, T. A. C. M, and Mecklenbrauker, W. F. G., "The Wigner Distribution—A Tool for Time-Frequency Signal Analysis," *Philips Journal of Research,* Vol. 35, No. 3, 1980, pp. 217–249.

[19]George, V. V., "Frequency-Time Spectral Analysis of Helicopter Turbulence and Response in Forward Flight," M.S. Thesis, Florida Atlantic Univ., Boca Raton, FL, Dec. 1990.

[20]George, V. V., Gaonkar, G. H., Prasad, J. V. R., and Schrage, D. P., "On the Adequacy of Modeling Turbulence and Related Effects on Helicopter Response," *Proceedings of the American Helicopter Society Technical Specialists' Meeting on Rotorcraft Basic Research,* Georgia Inst. of Technology, Atlanta, GA, March 1990.

[21]Gradshteyn, I. S., and Ryzhik, I. M., *Tables of Integrals, Series, and Products,* Academic Press, New York, 1980, p. 494.

[22]Madhavan, R., "Effects of Rotating Frame Turbulence and Dynamic Stall on Gust Response of Helicopter Blades," M.S. Thesis, Florida Atlantic Univ., Boca Raton, FL, April 1990.